



## OPEN ACCESS

## EDITED BY

Dmitry Aleksandrovich Zinovkin,  
Gomel State Medical University, Belarus

## REVIEWED BY

Andrei S. Babenka,  
Republican Research and Practical Center  
"Cardiology", Belarus  
Елена Франциянц,  
ФГБ, Russia

## \*CORRESPONDENCE

Xuehan Bi

✉ bxh2022@163.com

Xiaolei Liang

✉ liangxl07@lzu.edu.cn

Yongxiu Yang

✉ yxyanglzu@163.com

<sup>†</sup>These authors have contributed equally to  
this work

RECEIVED 19 August 2025

REVISED 10 November 2025

ACCEPTED 12 November 2025

PUBLISHED 26 November 2025

## CITATION

Chen X, Wu R, Wang Z, Wang F, Hu D, Bi X,  
Liang X and Yang Y (2025) Pan-cancer multi-  
omics characterization of calcyphosine and  
its revealed links to the immune  
microenvironment and regulatory  
networks in endometrial carcinoma.  
*Front. Immunol.* 16:1688606.  
doi: 10.3389/fimmu.2025.1688606

## COPYRIGHT

© 2025 Chen, Wu, Wang, Wang, Hu, Bi, Liang  
and Yang. This is an open-access article  
distributed under the terms of the [Creative  
Commons Attribution License \(CC BY\)](#). The  
use, distribution or reproduction in other  
forums is permitted, provided the original  
author(s) and the copyright owner(s) are  
credited and that the original publication in  
this journal is cited, in accordance with  
accepted academic practice. No use,  
distribution or reproduction is permitted  
which does not comply with these terms.

# Pan-cancer multi-omics characterization of calcyphosine and its revealed links to the immune microenvironment and regulatory networks in endometrial carcinoma

Xi Chen<sup>1†</sup>, Ruiyue Wu<sup>1†</sup>, Zijing Wang<sup>2</sup>, Fengfeng Wang<sup>3</sup>,  
Dan Hu<sup>4</sup>, Xuehan Bi<sup>4\*</sup>, Xiaolei Liang<sup>4\*</sup> and Yongxiu Yang<sup>4\*</sup>

<sup>1</sup>The First Clinical Medical College of Lanzhou University, Lanzhou, Gansu, China, <sup>2</sup>The First Clinical  
Medical College, General Hospital of Ningxia Medical University, Yinchuan, China, <sup>3</sup>Department of  
Surgery, Wushan Hospital of Traditional Chinese Medicine, Tianshui, Gansu, China, <sup>4</sup>Department of  
Obstetrics and Gynecology, The First Hospital of Lanzhou University, Lanzhou, Gansu, China

**Objective:** The calcium-dependent activator protein for secretion (CAPS) has emerged as a protein of interest in tumor biology; however, its functional significance in endometrial carcinoma (EC) remains largely unexplored.

**Methods:** We performed an integrative analysis leveraging bulk RNA sequencing data from The Cancer Genome Atlas, GTEx, and publicly available EC datasets, coupled with gene set enrichment analysis (GSEA) and single-cell transcriptomic profiling. The association between CAPS expression and clinicopathological parameters as well as patient prognosis was systematically assessed. In addition, functional enrichment, intercellular communication, and immune infiltration analyses were conducted to elucidate the molecular and microenvironmental roles of CAPS. *In vitro* assays were employed to validate the biological effects of CAPS knockdown on EC cell proliferation, migration, and invasion.

**Results:** CAPS was significantly upregulated in early-stage, low-grade, and endometrioid endometrial carcinoma, and its elevated expression was associated with improved patient survival. GSEA indicated that high CAPS expression was correlated with enhanced ribosome biogenesis and oxidative phosphorylation, along with suppression of proliferative signaling, reflecting a metabolically differentiated phenotype. Single-cell transcriptomic analysis revealed that CAPS was specifically enriched in terminally differentiated secretory epithelial cells, promoting epithelial maturation and oxidative metabolism. Furthermore, CAPS-positive cells exhibited extensive crosstalk with immune cells, suggesting a potential role in facilitating anti-tumor immune responses. Functional assays confirmed that CAPS knockdown markedly enhanced EC cell proliferation, migration, and invasion.

**Conclusion:** CAPS may act as a tumor suppressor in EC by stabilizing microtubule architecture, reprogramming cellular metabolism, and modulating immune interactions within the tumor microenvironment. These findings highlight CAPS as a promising prognostic biomarker and potential therapeutic target in EC.

#### KEYWORDS

CAPS, pan-cancer, endometrial carcinoma, multi-omics, immune remodeling

## 1 Background

Endometrial cancer (EC) is among the most prevalent gynecological malignancies, with an estimated lifetime risk of approximately 3.1% among women. Although most cases are diagnosed at an early stage (stage I) with a 5-year overall survival (OS) rate of 85%–90% (1), prognosis drops sharply to about 18% once distant metastasis develops. Current treatments including surgery, radiotherapy, and chemotherapy (2) form the cornerstone of EC management but are associated with significant limitations. Surgery is restricted to early-stage disease, radiotherapy is constrained by dose-limiting toxicity, nearly 40% of advanced cases develop resistance to chemotherapy, and immunotherapy shows clinical benefit primarily in microsatellite instability-high (MSI-H) or mismatch repair-deficient (dMMR) subtypes, with an objective response rate of only ~40% (3). Moreover, the pronounced molecular heterogeneity of EC further compromises the efficacy of conventional therapies and underscores the urgent need for reliable prognostic biomarkers and actionable therapeutic targets to facilitate precision medicine (4).

Calcyphosine (CAPS) is an EF-hand  $\text{Ca}^{2+}$ -binding phosphoprotein originally identified as a cAMP-dependent substrate in thyroid tissue; recent studies have drawn attention to its relevance in cancer biology. Through its EF-hand domains (Figure 1), CAPS binds  $\text{Ca}^{2+}$  and orchestrates calcium-dependent vesicle fusion and neurotransmitter release (4). Increasing evidence indicates aberrant CAPS expression across multiple cancers (5–8), implicating it in oncogenic signaling (9). Dysregulation of EF-hand-mediated calcium signaling and altered vesicular secretion may reshape the tumor microenvironment and modulate immune cell infiltration, suggesting a dual role for CAPS in calcium signaling and immune remodeling in EC (10).

In this study, we systematically characterized the molecular and clinical significance of CAPS across pan-cancer datasets by integrating The Cancer Genome Atlas (TCGA), GTEx, and Clinical Proteomic Tumor Analysis Consortium (CPTAC) multi-omics resources. Using single-cell transcriptomics, we delineated the cellular distribution and regulatory networks of CAPS within the EC tumor microenvironment. Finally, analyses of clinical samples and *in vitro* assays validated the biological role of CAPS in EC progression. Collectively, these findings identify CAPS as a

putative tumor suppressor, establish its prognostic value, and provide a foundation for CAPS-based diagnostic and therapeutic strategies.

## 2 Methods

### 2.1 Data sources and preprocessing

An overview of the datasets and sample information used in this study is provided in **Supplementary Table 1**. Gene expression profiles were obtained from the UCSC Xena database (<https://xenabrowser.net/>), which provides batch-corrected and normalized TCGA pan-cancer datasets as well as GTEx (11) normal tissue data. Protein expression profiles across multiple cancer types were retrieved from the CPTAC database (<https://proteomics.cancer.gov/programs/cptac>). Clinical characteristics and survival information for EC patients were downloaded from the TCGA portal (<https://portal.gdc.cancer.gov>). Genomic alterations of CAPS were analyzed using the cBioPortal platform (<https://www.cbioportal.org/>). Single-cell RNA sequencing data were obtained from the GEO database (<https://www.ncbi.nlm.nih.gov/geo/>), specifically dataset GSE173682 ( $n = 5$ ). The clinical characteristics of the endometrial carcinoma samples included in this dataset are summarized in **Supplementary Table 2**.

### 2.2 Expression and variation analysis

To assess differential expression of CAPS between tumor and normal tissues, Wilcoxon rank-sum tests were applied to compare mRNA levels. These findings were validated at the protein level using CPTAC data with the same statistical approach. CAPS expression across human organs was visualized using the R package *gganatomogram* (v1.1.1). Genomic alterations, including mutation frequency, mutation types, and copy number alterations (CNA), were analyzed using cBioPortal (<http://www.cbioportal.org>). Correlations between CAPS expression and tumor mutational burden (TMB) or microsatellite instability (MSI) were calculated using the R package *TCGApilot* (v8.0.0) with Pearson correlation analysis. All tests were two-sided, with  $P < 0.05$  considered statistically significant.

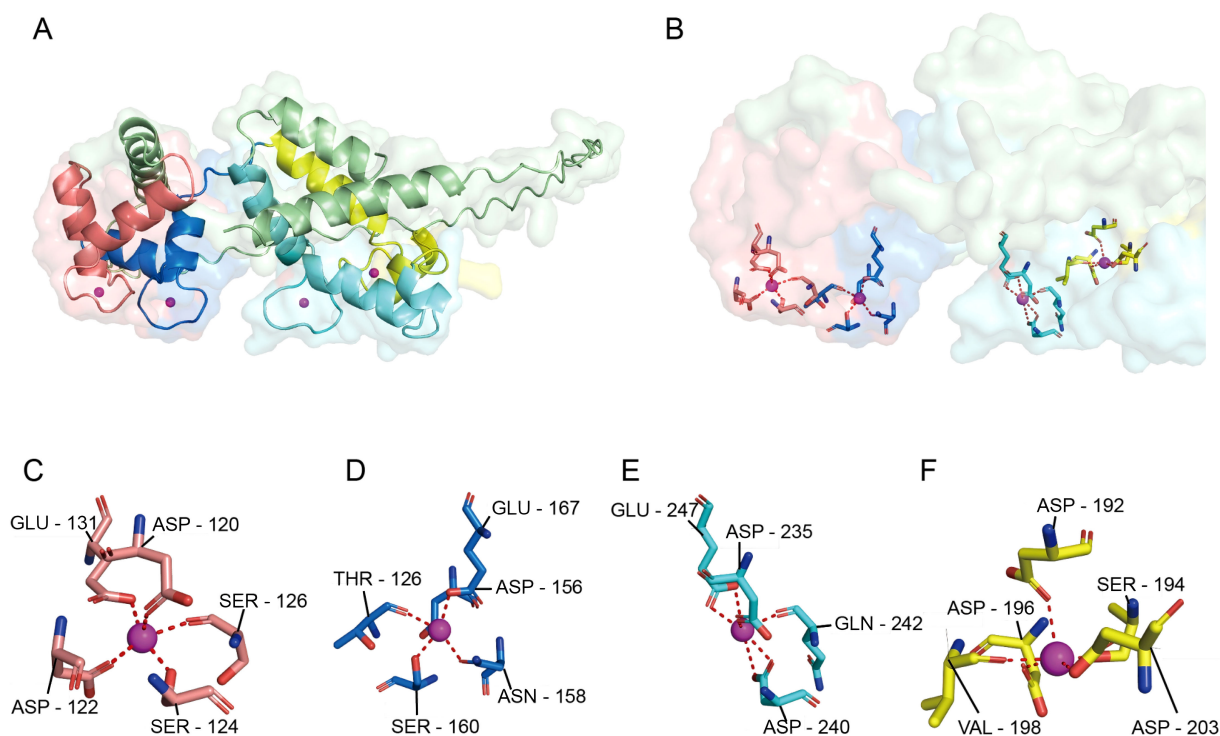


FIGURE 1

Surface conformation of CAPS and the four  $\text{Ca}^{2+}$ -binding pockets. (A) Overall schematic of the CAPS monomer, showing its characteristic bilobal structure consisting of an N-terminal lobe (EF1-EF2) and a C-terminal lobe (EF3-EF4). (B)  $\text{Ca}^{2+}$ -binding environment of the four EF-hand domains. Upon  $\text{Ca}^{2+}$  coordination, the C-lobe (light cyan) undergoes a pronounced conformational change forming a prominent hydrophobic pocket, while the N-lobe (light red) is partially shielded by an additional  $\alpha$ -helix (yellow), limiting access to its binding site. (C–F) Coordination details of EF-hands 1–4. Each site adopts a typical seven- or eight-coordination geometry, primarily mediated by oxygen atoms from Asp/Glu residues (dashed lines indicate  $\text{Ca}^{2+}$ -ligand distances). EF1 (C) and EF2 (D) reside within the N-terminal lobe, while EF3 (E) and EF4 (F) are located in the C-terminal lobe, collectively enabling the  $\text{Ca}^{2+}$ -dependent conformational regulation of CAPS.

## 2.3 Pan-cancer survival and clinical outcome analysis

The prognostic relevance of CAPS expression across cancers was evaluated using the R packages survival (v3.6-4) and survminer (v0.5.0). Associations with OS, progression-free interval (PFI), and disease-specific survival (DSS) were systematically assessed. Kaplan-Meier survival curves were generated, and group differences were tested by log-rank tests. Univariate Cox proportional hazards regression models were applied to estimate the protective or risk effects of CAPS expression (12), with hazard ratios (HRs) and 95% confidence intervals (CIs) reported. Forest plots were generated using the forestplot package (v2.0.1) to visualize HRs and CIs across cancer types. All analyses were two-sided, with  $P < 0.05$  considered significant.

## 2.4 CAPS expression, clinicopathological characteristics, and prognostic model analysis in endometrial cancer

In EC, we used the Kruskal-Wallis nonparametric test (does not require normal distribution) to assess the association between CAPS expression [ $\log_2(\text{TPM} + 1)$ ] and clinicopathological

characteristics (age, histological type, residual tumor status) ( $P < 0.05$ ), as gene expression data often deviate from normality due to biological heterogeneity, unequal variances, and small sample sizes, and this test ensures robust inter-group comparisons. To determine the independent prognostic value of CAPS, univariate and multivariate Cox regression analyses were conducted alongside relevant clinical variables. Based on these results, a nomogram model was constructed to predict OS, with calibration curves used to assess predictive accuracy. A nomogram-based prognostic tool was subsequently developed to facilitate individualized survival prediction (13). The concordance index (C-index) (14) was used to quantify the predictive ability of the nomogram. Calibration analysis and visualization were performed using the 'rms' (v8.0.0) package. All analyses were performed in R (v4.2.1), with two-sided  $P < 0.05$  considered statistically significant.

## 2.5 Functional enrichment and multi-omics analysis of CAPS and immune infiltration

To explore the molecular mechanisms of CAPS-related pathways in EC, genome-wide Pearson correlation analysis was performed using the psych package. Genes significantly co-expressed with CAPS ( $|\text{Cor}| > 0.5$ ,  $P < 0.05$ ) were identified (15)

and subjected to Gene Ontology (GO; biological process, molecular function, and cellular component) and KEGG pathway enrichment analyses using cluster Profiler (v4.10.0) (16). Gene set enrichment analysis (GSEA) was further conducted with 1,000 permutations based on the Hallmark gene sets from MSigDB (<https://www.gsea-msigdb.org/gsea/msigdb>). To assess the association between CAPS expression and immune infiltration, two complementary approaches were applied: the ssGSEA algorithm implemented in GSVA (v1.46.0) and the CIBERSORT deconvolution algorithm (v1.06) (17). Marker genes from 24 immune cell types in EC and 22 immune cell types across pan-cancer cohorts were analyzed. Results were visualized with ggplot2 (v3.4.3), Complex Heatmap (v2.16.0), and other R packages.

## 2.6 Single-cell transcriptomic analysis

Single-cell transcriptomic analyses were performed in R (v4.2.1). Raw sequencing data were processed and quality-controlled using Seurat (v5.1.0). Criteria included retention of genes expressed in at least three cells, exclusion of cells with >10% mitochondrial content, and removal of low-quality cells with <300 or >5,000 detected genes. Batch effects were corrected using the Harmony algorithm (v0.1.1) (18). Cell clusters were annotated based on canonical marker gene expression and manually validated. Intercellular communication networks were inferred with CellChat (v1.6.1) using the human ligand-receptor database (19). Stemness features were quantified with CytoTRACE (v0.3.3), and developmental trajectories were reconstructed to model differentiation dynamics. Using the Monocle package (v2.28.0) to construct time-series trajectories of SEC cells, tracking their dynamic changes during development.

## 2.7 Clinical sample collection

We collected paired clinical tissue specimens from 12 patients with pathologically confirmed primary endometrioid EC. Each patient provided both tumor tissue (Cancer,  $n = 12$ ) and matched adjacent noncancerous tissue (Normal,  $n = 12$ ). Eligible patients had complete clinicopathological data, received no preoperative radiotherapy, chemotherapy, or hormonal therapy, and had no history of other malignancies or severe systemic disease. The “adjacent noncancerous tissue (NC)” was defined as histologically normal endometrium located at least 2 cm from the tumor margin, and all NC samples were pathologically reviewed to exclude microscopic infiltration. For experimental procedures, formalin-fixed, paraffin-embedded (FFPE) tissues were used for immunohistochemistry, with surgical specimens fixed in 10% neutral-buffered formalin for approximately 24 h at room temperature, processed, and paraffin-embedded according to standard pathology protocols; blocks were stored at room temperature in a desiccated environment until sectioning. Fresh-frozen tissues were used for Western blotting: each specimen was snap-frozen in liquid nitrogen within 30 min of resection and stored

at  $-80^{\circ}\text{C}$ . For protein extraction, frozen tissues were homogenized in RIPA lysis buffer (Solarbio, Beijing, China) supplemented with phenylmethylsulfonyl fluoride (PMSF; Solarbio, Beijing, China) and a protease inhibitor cocktail (Beyotime, Shanghai, China). The homogenate was centrifuged at  $12,000 \times g$  for 10 min at  $4^{\circ}\text{C}$ , and the supernatant was collected. Protein concentration was determined using a BCA assay (Solarbio, Beijing, China), followed by Western blot analysis.

## 2.8 Immunohistochemistry

We performed IHC on FFPE sections ( $4 \mu\text{m}$ ). After dewaxing and rehydration, sections underwent heat-induced antigen retrieval in citrate buffer (pH 6.0) for 15 minutes, followed by blocking with 0.3% hydrogen peroxide ( $\text{H}_2\text{O}_2$ ) and normal goat serum. Sections were incubated overnight at  $4^{\circ}\text{C}$  with anti-CAPS antibody (Abmart, PK35981; 1:200), then with an HRP-conjugated secondary antibody, developed with DAB (BOSTER, China), and counterstained with hematoxylin. For quantification, one slide per case was scanned; three representative high-power fields ( $\times 200$ ) were analyzed in ImageJ to calculate mean optical density ( $\text{MOD} = \text{integrated optical density [IOD]}/\text{area}$ ), and the mean of the three fields was taken as the final MOD for each case. CAPS staining localized predominantly to the cytoplasm. Two pathologists, blinded to group labels, independently scored the slides; if the inter-rater MOD differed by >10%, discrepancies were resolved by joint review. Antibody validation: using the same antibody in Western blotting, a single specific band at  $\sim 20\text{--}21 \text{ kDa}$  was detected, supporting antibody specificity under our conditions.

## 2.9 Western blot analysis

We performed Western blot analysis on all 12 cases of Cancer and Normal tissue. For each sample,  $20 \mu\text{g}$  of total protein was separated on 10% SDS-PAGE gels and transferred to PVDF membranes. The membranes were blocked with 5% skim milk, incubated with anti-CAPS primary antibody (Abmart, catalog no. PK35981 1:1000) and anti- $\beta$ -actin (1:5000, Servicebio, Cat.#G1213) primary antibody (internal control), followed by incubation with horseradish peroxidase (HRP)-labeled secondary antibody. Images were developed and captured using ECL chemiluminescence. Density quantification was performed using ImageJ software, with CAPS band intensity normalized against  $\beta$ -actin. All results are derived from 3 independent biological replicates.

## 2.10 Cell culture

The human EC cell lines KLE and Ishikawa were obtained from GeneChem Co., Ltd. (Shanghai, China). Ishikawa cells were cultured in Dulbecco's Modified Eagle Medium (DMEM; Hyclone, Logan, UT, USA) supplemented with 10% fetal bovine serum (FBS; Siji Green, China) and 1% penicillin-streptomycin (Servicebio, Wuhan,



China). KLE cells were maintained in DMEM/F12 medium (Hyclone, Logan, UT, USA) supplemented with 10% FBS and 1% penicillin–streptomycin. All cells were incubated at 37°C in a humidified atmosphere containing 5% CO<sub>2</sub>.

## 2.11 Cell transfection

Ishikawa and KLE cells were transfected with CAPS-targeting small interfering RNAs (siRNAs; siRNA-CAPS) or a non-silencing control (Si-NC) according to the manufacturer's protocol. Three independent siRNAs (Si1-CAPS, Si2-CAPS, and Si3-CAPS), along with the negative control (Si-NC), were synthesized by Hanbio Biotechnology Co., Ltd. (Shanghai, China), and their sequences are provided in [Supplementary Table 4](#). Cells were seeded in six-well plates at a density of  $1 \times 10^5$  cells/mL in 2 mL complete medium per well. When cell confluence reached ~50%, transfection was performed using Lipofectamine 8000 (Invitrogen, USA). Following transfection, cells were maintained under standard conditions (37°C, 5% CO<sub>2</sub>) for 48 h before subsequent assays.

## 2.12 CCK-8 cell proliferation assay

Cell proliferation was evaluated using the Cell Counting Kit-8 (CCK-8; BioScience, China) in Ishikawa and HEC-1-A cells. Cells were seeded into 96-well plates at a density of  $5 \times 10^3$  cells per well and cultured for 0, 24, 48, and 72 hours. At each time point, cell morphology was examined under a microscope before reagent addition to avoid artifacts. Then, 10 µL of CCK-8 reagent was added to each well and incubated at 37°C in the dark for 2 hours. The absorbance at 450 nm (OD<sub>450</sub>) was measured using a microplate reader (Thermo Scientific, USA). OD<sub>450</sub> values were normalized to the control group (Si-NC) at each time point. Each experiment included three biological replicates, with technical triplicates per condition. Statistical analysis was performed using two-tailed unpaired Student's t-tests.

## 2.13 EdU staining assay

EdU incorporation assays were performed using the Cell-Light™ EdU Apollo567 *In Vitro* Kit (RiboBio, China) in Ishikawa and KLE cells. Cells were seeded into 24-well plates containing coverslips and incubated with 50 µM EdU for 2 h at 37°C. Before fixation, cell morphology and confluence were inspected microscopically to ensure uniform growth. Cells were then fixed with 4% paraformaldehyde, permeabilized with 0.5% Triton X-100, and stained with the Apollo567 reaction cocktail followed by DAPI counterstaining. Images were captured using a fluorescence microscope (Revvity, USA). For each well, three randomly selected fields (×200) were analyzed using ImageJ software, with consistent thresholds for EdU and DAPI channels. The EdU labeling index (%) =  $\text{EdU}^+ \text{ cells} / \text{DAPI}^+ \text{ cells} \times 100$ . Each experiment included three biological replicates, each with

technical triplicates. Statistical analysis was performed using two-tailed unpaired Student's t-tests.

## 2.14 Wound healing assay

Cell migration was assessed using a wound-healing assay in Ishikawa and KLE cells. Cells were seeded into six-well plates and cultured until reaching full confluence. A sterile 200 µL pipette tip was used to create a vertical scratch across the monolayer. Detached cells were removed by PBS washing, and serum-free medium was added. Cell morphology was examined immediately after scratching to ensure smooth wound edges and to avoid artifacts. Images of the wound area were captured at 0, 24, and 48 h using an inverted microscope (×100). Three randomly selected fields per well were analyzed using ImageJ software, and the percentage of wound closure was calculated as  $(A_0 - A_t) / A_0 \times 100\%$ , where  $A_0$  and  $A_t$  represent the initial and residual wound areas, respectively. Each experiment was performed in triplicate with three independent biological replicates. Statistical analyses were conducted using two-tailed unpaired Student's t-tests.

## 2.15 Transwell migration and invasion assays

Cell migration and invasion were evaluated using Transwell chambers (8 µm pore size, Corning, USA) in Ishikawa and KLE cells. Transfected cells were resuspended in serum-free DMEM at a density of  $8 \times 10^4$  cells/200 µL and seeded into the upper chambers, while the lower chambers were filled with 700 µL medium containing 20% fetal bovine serum as a chemoattractant. For invasion assays, the upper chambers were pre-coated with Matrigel (BD Biosciences, USA). After 24 h incubation at 37°C, non-migrated cells on the upper membrane surface were gently removed. Cells that had migrated or invaded to the lower surface were fixed with 4% paraformaldehyde, stained with 0.5% crystal violet in methanol (Solarbio, China) for 30 min, and examined microscopically to confirm consistent staining and morphology. Five randomly selected fields (×200) per insert were imaged, and the number of migrated or invaded cells was quantified using ImageJ software. Each assay was conducted in triplicate with three independent biological replicates, and two-tailed unpaired Student's t-tests were used for statistical analysis.

## 2.16 Statistical analysis

All statistical analyses were performed using GraphPad Prism 9.0 (GraphPad Software, USA). Continuous variables were expressed as mean ± standard error of the mean (SEM), and categorical variables as frequencies and percentages. Data normality was assessed using the Shapiro-Wilk test. Comparisons between two groups were conducted using two-tailed unpaired Student's t-tests for normally distributed data or Mann-Whitney U tests for non-normal data. For multiple

group comparisons, one-way ANOVA (for normal data) or Kruskal-Wallis tests (for non-normal data) were applied, with Bonferroni *post-hoc* correction when appropriate. Correlations were analyzed using Pearson's correlation coefficient. Statistical significance was defined as \*\*\* $P < 0.001$ , \*\* $P < 0.01$ , and \* $P < 0.05$ . Each experiment was independently repeated at least three times to ensure reproducibility.

## 3 Result

### 3.1 Multi-omics analysis of CAPS expression, sex-specific differences, and prognostic value across pan-cancer

By integrating transcriptomic data from TCGA and proteomic data from the CPTAC, we observed that CAPS exhibits consistently aberrant expression patterns across multiple malignancies. Specifically, elevated CAPS expression was detected in 11 cancer types, including uterine corpus endometrial carcinoma (UCEC), breast invasive carcinoma (BRCA), and ovarian cancer (OV) (Figures 2A, B). Prognostic analyses based on OS, PFI, and DSS demonstrated that CAPS exhibits distinct prognostic implications across cancer types (Figures 2E–G). Notably, high CAPS expression was associated with favorable prognosis in UCEC (HR = 0.46, 95% CI: 0.29–0.72,  $P < 0.001$ ), but correlated with poor survival outcomes in lower-grade glioma (LGG) (HR = 2.39, 95% CI: 1.69–3.38,  $P < 0.001$ ). These findings were further validated by Kaplan-Meier survival analyses (Supplementary Figures S1A–H). Collectively, these multi-omics and multi-cohort analyses highlight the context-dependent role of CAPS across tumor types and underscore its potential utility as a molecular biomarker for precision oncology.

### 3.2 Genomic landscape of CAPS

To systematically elucidate the molecular characteristics of CAPS, we first mapped its genomic location to chromosome 19q13.1–q13.2 (Supplementary Figure S2A). Pan-cancer mutation profiling using TCGA data revealed an overall alteration frequency of 0.9%, with copy number amplification as the predominant event, followed by deep deletion (Figure 3A). Notably, hotspot mutations V157G and X157\_splice, located within the EF-hand calcium-binding domain, may impair CAPS's  $\text{Ca}^{2+}$ -binding capacity (Figure 3B). Genomic Identification of Significant Targets in Cancer (GISTIC) analysis further demonstrated a gene dosage effect, as CAPS mRNA expression was significantly elevated in gain/amplification groups and reduced in shallow/deep deletion groups (Figure 3C). Tissue-specific alteration patterns were also observed: copy number amplification predominated in sarcoma and lower-grade glioma, whereas deep deletions were more frequent in UCEC (Figure 3D). These findings suggest that CAPS loss may contribute to EC progression, potentially functioning as a tumor suppressor. However, due to the relatively low overall mutation frequency, the precise mechanisms remain to be elucidated.

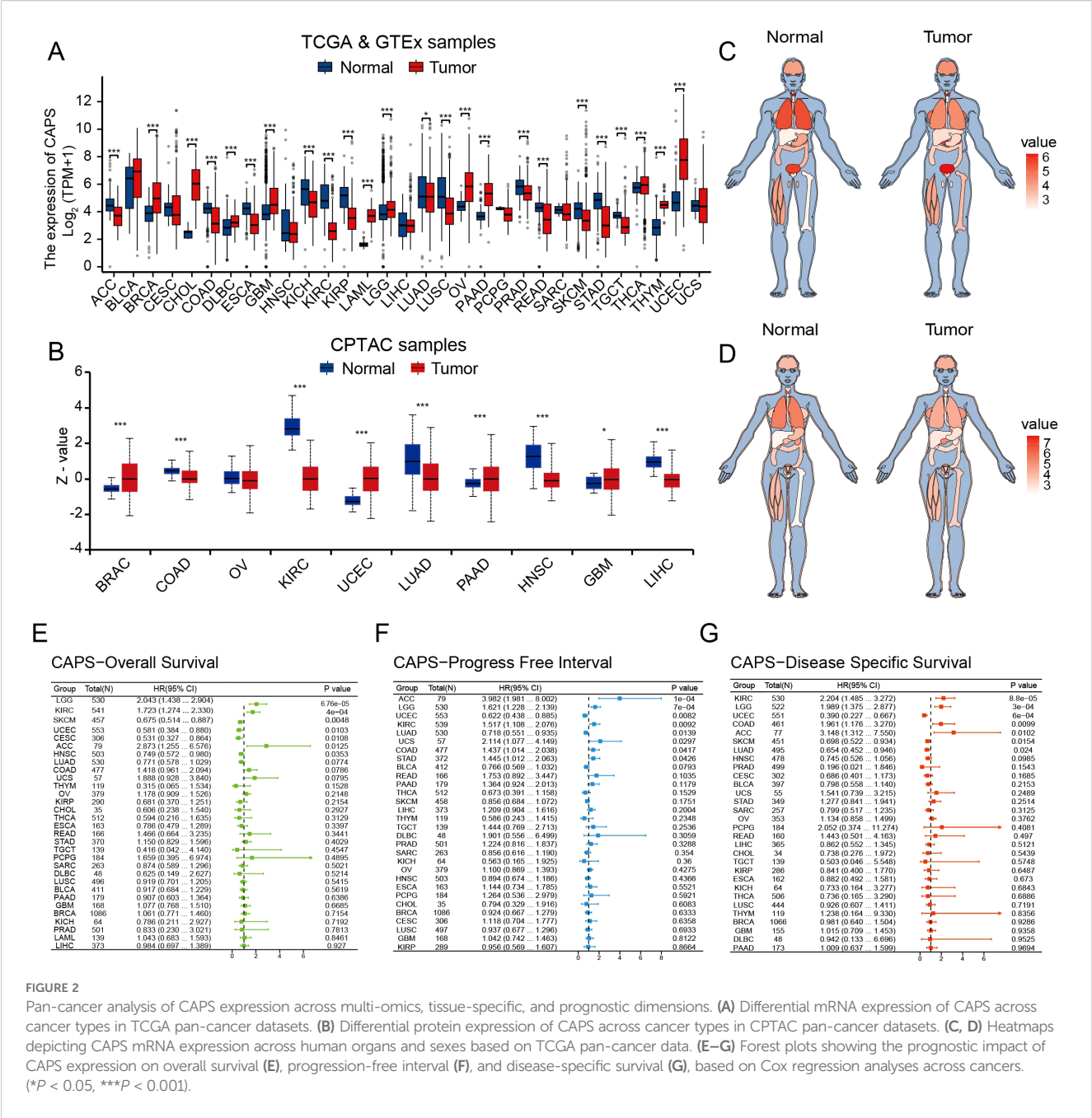
We next evaluated the correlation between CAPS expression and TMB as well as MSI, revealing tumor-type-specific associations. CAPS expression was positively correlated with TMB in glioblastoma but negatively correlated in gastric and colon cancers (Figure 3E). Similarly, it was positively associated with MSI in chromophobe renal cell carcinoma and negatively in uterine carcinosarcoma (Figure 3F). Importantly, in EC, CAPS expression did not show significant correlations with either TMB or MSI, suggesting its role in tumorigenesis may involve alternative, non-mutational pathways. Collectively, these results underscore the molecular heterogeneity of CAPS alterations across different tumor types and highlight the need for further mechanistic studies in specific tumor contexts.

### 3.3 Association of CAPS expression with clinicopathological features and prognosis in EC

Based on clinical data from the TCGA-UCEC cohort, CAPS expression was significantly associated with key clinicopathological features and patient prognosis in EC (Figures 4A–H). Elevated CAPS expression was observed in patients aged  $\leq 60$  years, those with stage I, histological grade G1, myometrial invasion  $< 50\%$ , and endometrioid histology. In contrast, CAPS expression was markedly reduced in high-grade tumors (G2–G3), serous carcinoma, advanced-stage disease (stage III–IV), and tumors with deep myometrial invasion (all  $P < 0.05$ ). These findings indicate that CAPS is preferentially expressed in early-stage, low-grade, and superficially invasive tumors, consistent with an indolent tumor phenotype and favorable clinical outcomes. To further assess the prognostic relevance of CAPS, a Cox proportional hazards model was constructed using overall survival data from 553 TCGA-UCEC patients. Univariate Cox regression identified high CAPS expression as a protective factor (HR = 0.87, 95% CI: 0.80–0.94,  $P = 0.002$ ) (Figure 4I). However, its independent prognostic significance was diminished in multivariate analysis after adjustment for established clinical variables (adjusted HR = 0.92, 95% CI: 0.78–1.07,  $P = 0.32$ ) (Figure 4J). Given the biological importance of CAPS and its complementary predictive value, we integrated CAPS expression with seven clinicopathological variables to construct a prognostic nomogram for UCEC patients (Figure 4K). This model provided an intuitive tool for estimating 1- and 3-year survival probabilities. The calibration curves demonstrated strong concordance between predicted and observed outcomes (C-index = 0.82; Figure 4L), supporting CAPS holds significant reference value for the clinical evaluation of patients with EC.

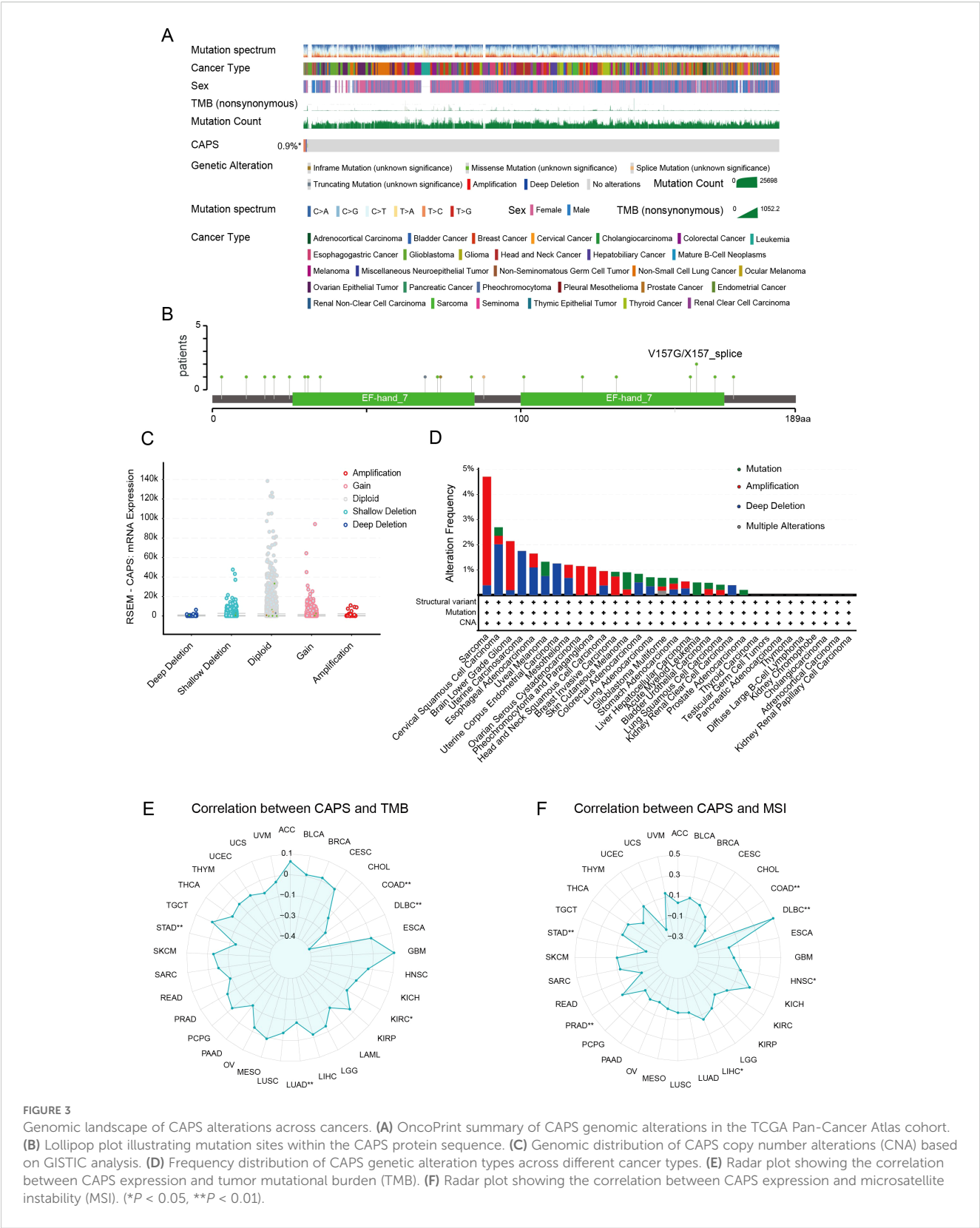
### 3.4 Expression features of CAPS in the EC microenvironment and functional enrichment analysis

Based on single-cell transcriptomic analysis of the GSE173682 dataset from GEO, we systematically characterized the expression profile of CAPS within the EC microenvironment. Following



stringent quality control to retain high-quality cells (Supplementary Figures S3A–C), fifteen significant principal components were identified via elbow plot analysis (Supplementary Figure S3D). Clustering at a resolution of 1.2 yielded 24 robust clusters (Supplementary Figures S3E, F), and UMAP visualization (Figures 5A, B) delineated ten major cell types, including epithelial cells, fibroblasts, endothelial cells, and various immune cell populations. Analysis of cellular composition across samples revealed marked inter-individual heterogeneity (Supplementary Figure S3G), likely reflecting dynamic alterations within the tumor microenvironment. Notably, CAPS expression exhibited pronounced cell-type specificity, being markedly enriched in secretory endometrial epithelial cells (SecECs) relative to other cell types (Figure 5C,

Supplementary Figure S3H). Sub-clustering of SecECs with optimized parameters (Supplementary Figure S3I) identified five functional subpopulations (Figure 5D, Supplementary Figure S3J): stem/progenitor-like, highly proliferative, inflammatory secretory, specialized differentiated, and stress-associated inflammatory subsets. Expression density mapping (Figure 5E) revealed that CAPS expression peaked in the specialized differentiated subgroup (neuroendocrine-like cells), but was comparatively low in the proliferative and inflammation-associated clusters. CytoTRACE2 analysis of differentiation status (Figure 5F) showed a progressive increase in CAPS expression along the epithelial trajectory, peaking at terminal differentiation. Pseudotime analysis (Figure 5G) likewise indicated that CAPS expression tracks branch progression in SecECs.



Taken together, CAPS expression rises with epithelial maturation and is associated with a more differentiated secretory epithelial phenotype.

To further investigate the biological function of CAPS, we performed functional enrichment analysis of CAPS-related genes in the TCGA-UCEC cohort. Gene Ontology and KEGG pathway analyses demonstrated significant enrichment in processes such as cilium movement and tubulin binding, as well as metabolic pathways including ether lipid metabolism and fat digestion and



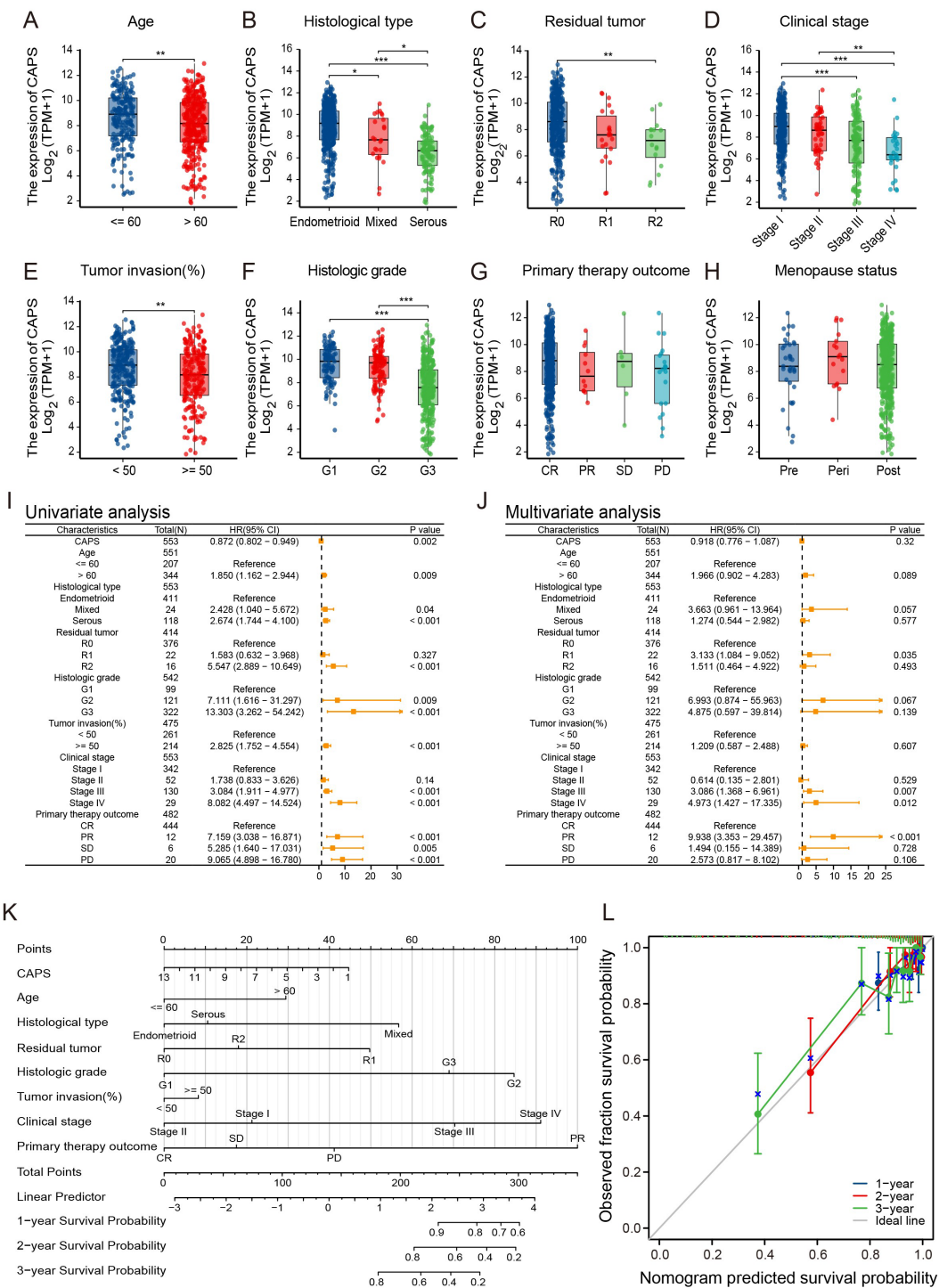


**FIGURE 4** Association of CAPS expression with clinicopathological features and prognosis in EC. (A–H) Correlation between CAPS expression levels and clinicopathological parameters in UCEC patients: (A) age, (B) histological subtype, (C) residual tumor status, (D) FIGO stage, (E) depth of myometrial invasion, (F) histological grade, (G) primary therapy outcome, and (H) menopausal status. (I, J) Univariate (I) and multivariate (J) Cox regression analyses of CAPS expression and clinical variables for overall survival. (K) Prognostic nomogram integrating CAPS expression and clinicopathological variables based on multivariate Cox model. (L) Calibration plot evaluating the performance of the prognostic nomogram. (ns,  $P \geq 0.05$ , \* $P < 0.05$ , \*\* $P < 0.01$ , \*\*\* $P < 0.001$ ).

absorption (Supplementary Figure S2B). Network visualization classified these into two functional modules: (1) a high-density cluster centered on “cilium movement/microtubule binding,” and (2) a metabolism-associated cluster focused on “ether lipid

metabolism/fat digestion and absorption” (Supplementary Figure S2C). GSEA enrichment analysis further revealed that CAPS-related genes were positively associated with ribosome biogenesis, oxidative phosphorylation, and  $\alpha$ -linolenic acid metabolism, while

negatively correlated with proliferative pathways such as cell cycle and DNA replication (Supplementary Figure S2D). Collectively, these results indicate that CAPS may influence EC progression through dual mechanisms: modulating microtubule or ciliary systems to regulate cellular motility, and reprogramming metabolic and cell cycle pathways to restrict aberrant proliferation.

### 3.5 Cell-cell communication features and immune-related functions of CAPS in the EC microenvironment

To further elucidate the role of CAPS in the tumor microenvironment of EC, we conducted a comprehensive cell-cell communication analysis using the previously described single-cell dataset. The intercellular communication network (Figures 6A, B) revealed both the number and strength of interactions between CAPS high-/low-expressing secretory endometrial epithelial cells (SecECs) and various immune microenvironmental cell types. Ligand-receptor pathway analysis (Figure 6C) identified the MDK-NCL and MIF-CD74 signaling axes as the principal routes through which CAPS high SecECs engaged in paracrine interactions. In these pathways, MDK and MIF ligands, secreted by CAPS high SecECs, mediated key signaling events with neighboring immune and stromal cells. Specifically, the most prominent targets of the MDK axis were NSecECs and mural cells, while the MIF pathway primarily engaged dendritic cells and natural killer (NK) cells (Figure 6D). Global communication profiling (Figure 6E) revealed mural cells as the most active signal transmitters, whereas NK cells served as the major recipients. Within the MDK pathway, CAPS high SecECs exhibited the most robust secretory activity, with NSecECs acting as the primary receiving population (Figure 6F). Complementary analysis using ssGSEA and CIBERSORT algorithms in the TCGA-UCEC and pan-cancer cohorts further supported these findings (Figure 6G). In EC, CAPS expression was positively correlated with the infiltration of NK cells ( $R = 0.421$ ), eosinophils ( $R = 0.301$ ), neutrophils ( $R = 0.146$ ), and T cells ( $R = 0.087$ ), but showed no significant association with regulatory T cells (Tregs) or B cells. Cell fraction analysis (Figure 6H) illustrated the distribution of CAPS expression across diverse immune subsets, although no definitive immunophenotypic bias was observed, likely due to the inherent limitations of bulk RNA sequencing. Importantly, pan-cancer analyses in additional tumor types, including bladder carcinoma (BLCA), clear cell renal cell carcinoma (KIRC), and colorectal adenocarcinoma (COAD), consistently demonstrated correlations between CAPS expression and immune microenvironment remodeling (Supplementary Figures S4F,G, Supplementary Figures S4A–K). Taken together, these results delineate the immunological functions and communication features of CAPS at both single-cell and transcriptomic levels, providing novel insights into its regulatory role within the tumor immune microenvironment.

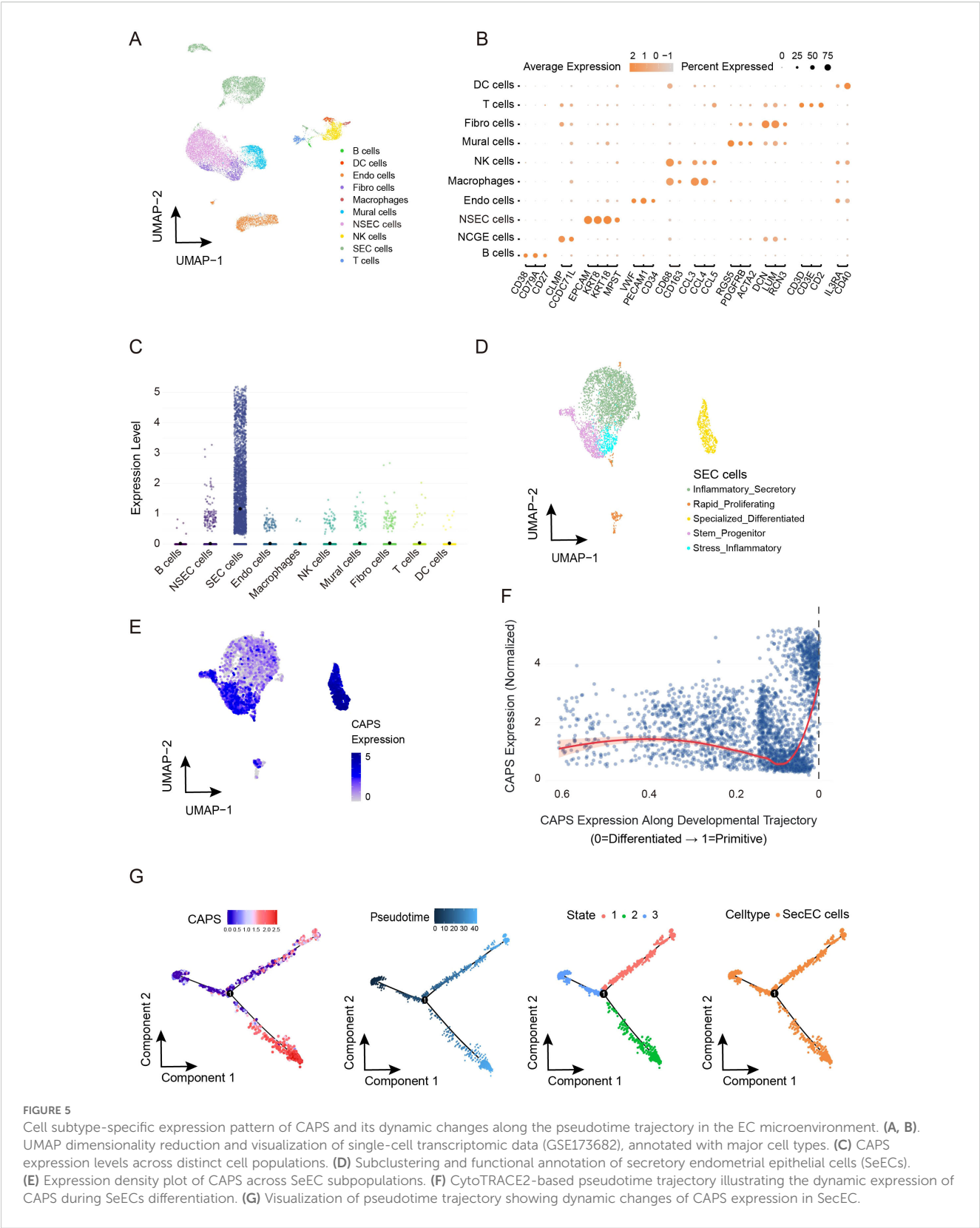
### 3.6 Downregulation of CAPS promotes proliferation, migration, and invasion of EC cells

To validate CAPS expression in EC, IHC and Western blot analyses were performed on tumor tissues and matched adjacent non-tumor tissues from EC patients. IHC staining revealed significantly higher CAPS expression in tumor tissues compared to adjacent non-tumor counterparts (Figures 7A–C). Quantitative Western blotting further confirmed elevated CAPS protein levels in tumor specimens ( $P < 0.01$ ; Figure 7D). We selected Ishikawa and KLE cells with high endogenous CAPS expression (Supplementary Table 3). Transfection with two independent siRNA sequences effectively silenced CAPS expression (Supplementary Table 4, Figure 7K). CCK-8 assays showed that optical density (OD<sub>450</sub>) values were significantly increased in CAPS-knockdown groups compared to controls at 48 h and 72 h ( $P < 0.05$ ; Figures 7E–G), suggesting enhanced cell viability. Consistently, EdU incorporation assays demonstrated a significant increase in EdU-positive cells following CAPS knockdown ( $P < 0.01$ ; Figures 7H–J), indicating accelerated DNA synthesis and cell proliferation. To assess the impact of CAPS on cell motility and invasiveness, wound healing and Transwell assays were performed. The wound healing assay revealed significantly enhanced wound closure in CAPS-silenced cells at 24 h ( $P < 0.01$ ; Figures 8A–D). Similarly, Transwell migration assays showed a marked increase in the number of migrating cells ( $P < 0.01$ ; Figures 8E–G), while Matrigel-coated invasion assays confirmed elevated invasive capacity following CAPS knockdown ( $P < 0.01$ ; Figures 8F–H). Collectively, these results demonstrate that silencing CAPS promotes EC cell proliferation, migration, and invasion *in vitro*. These findings support a tumor-suppressive role for CAPS in EC and suggest that CAPS may restrain malignant progression by limiting the aggressive phenotypes of EC cells.

## 4 Discussion

CAPS was initially identified in canine thyroid tissue as a calcium-dependent secretory activator protein harboring an EF-hand domain, classically associated with ion transport and thyroid function. However, its role in tumorigenesis remains largely undefined. In this study, we employed an integrative multi-omics approach, including pan-cancer genomic profiling and single-cell transcriptomic analysis, to comprehensively characterize the molecular and functional roles of CAPS in EC.

CAPS was found to be significantly upregulated in EC, with the highest expression levels observed in early-stage, low-grade, superficially invasive, and endometrioid-type tumors. Its elevated expression correlated strongly with favorable patient prognosis. Notably, CAPS expression progressively declined with advancing tumor stage, suggesting its potential role in restraining disease progression. Pan-cancer genomic analyses revealed that CAPS



transcription is primarily regulated by copy number variation, with frequent deep deletions observed in UCEC and uterine sarcoma. Co-expression and functional enrichment analyses indicated that CAPS may modulate tumor behavior by regulating the cilium–

microtubule system, cell cycle, and metabolic pathways—facilitating metabolic activation while restraining excessive proliferation to maintain a differentiated epithelial phenotype. Similarly, functional validation demonstrated that CAPS knockdown

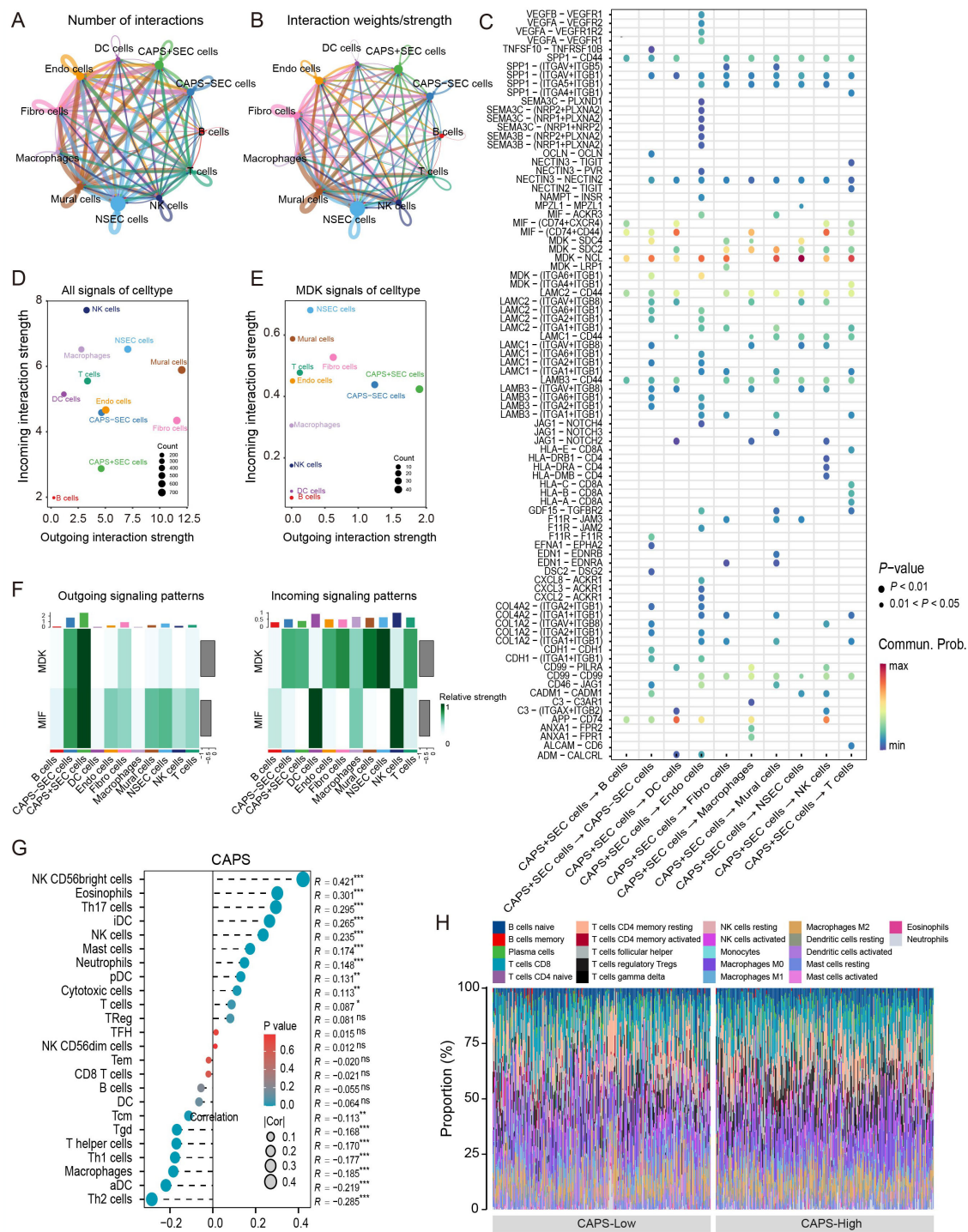


**FIGURE 6** Cell-cell communication features of CAPS in the tumor microenvironment of EC. **(A, B)** Intercellular interaction networks showing the number and weight of interactions between CAPS high/low-expressing SECs and other cell types. **(C)** Analysis of key ligand-receptor signaling pathways involved in CAPS-mediated intercellular communication. **(D, E)** Global communication landscape and CAPS-specific signaling activity via the MDK pathway. **(F)** Heatmap of differential signaling pathway activities across cell populations. **(G)** Pearson correlation analysis between CAPS expression and immune cell infiltration in the TCGA-UCEC cohort. **(H)** Proportional distribution of CAPS expression across various immune cell types. (\* $P < 0.05$ , \*\* $P < 0.01$ , \*\*\* $P < 0.001$ , ns: not significant).

markedly enhanced EC cell proliferation, migration, and invasion *in vitro*. As a calcium-binding protein, CAPS has been implicated in spindle apparatus organization and mitotic regulation (20). High CAPS expression appears to preserve cytoskeletal integrity and cellular quiescence, whereas its downregulation may lead to structural destabilization and uncontrolled cell cycle activation (21). Previous studies have linked primary cilia loss to



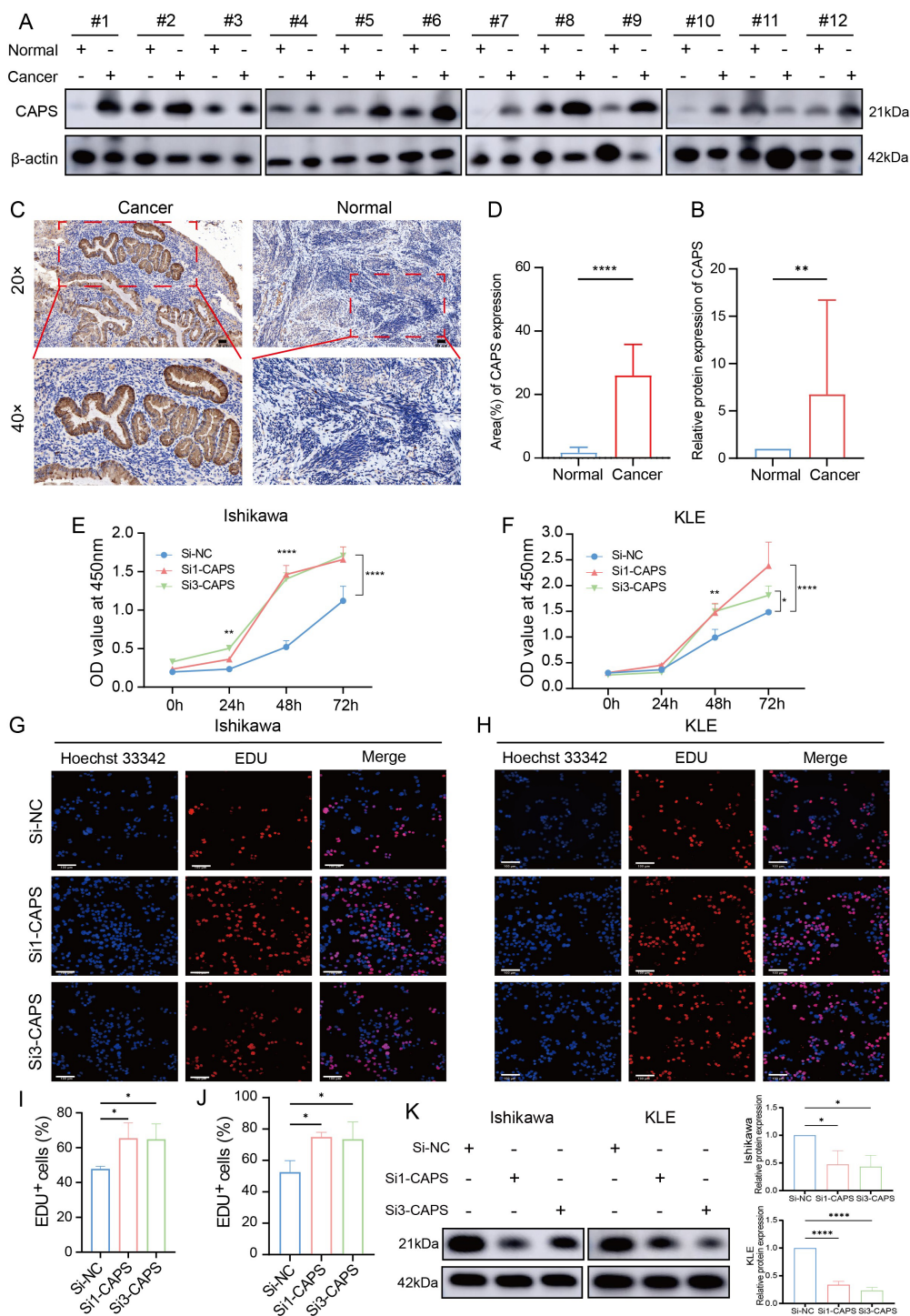


**FIGURE 7**  
CAPS expression in EC and its impact on cell proliferation. **(A)** Western blot analysis of CAPS protein levels in EC tissues and paired adjacent non-tumor tissues. **(B)** Quantification of CAPS protein expression based on Western blot results. **(C)** Representative immunohistochemical (IHC) staining images of CAPS in EC and adjacent tissues at 20x and 40x magnification. **(D)** Statistical analysis of IHC scores (n = 12 per group). **(E, F)** CCK-8 assays evaluating cell viability in KLE and Ishikawa cells following CAPS knockdown. **(G, H)** EdU staining assays assessing proliferative capacity after CAPS knockdown in KLE and Ishikawa cells. **(I, J)** Quantification of EdU-positive cells. **(K)** CAPS knockdown efficiency validated by Western blot in Ishikawa and KLE cells. CAPS protein levels were markedly reduced after transfection with Si1-CAPS and Si3-CAPS compared with Si-NC. β-actin served as the loading control. (\*P < 0.05, \*\*P < 0.01, \*\*\*\*P < 0.0001).

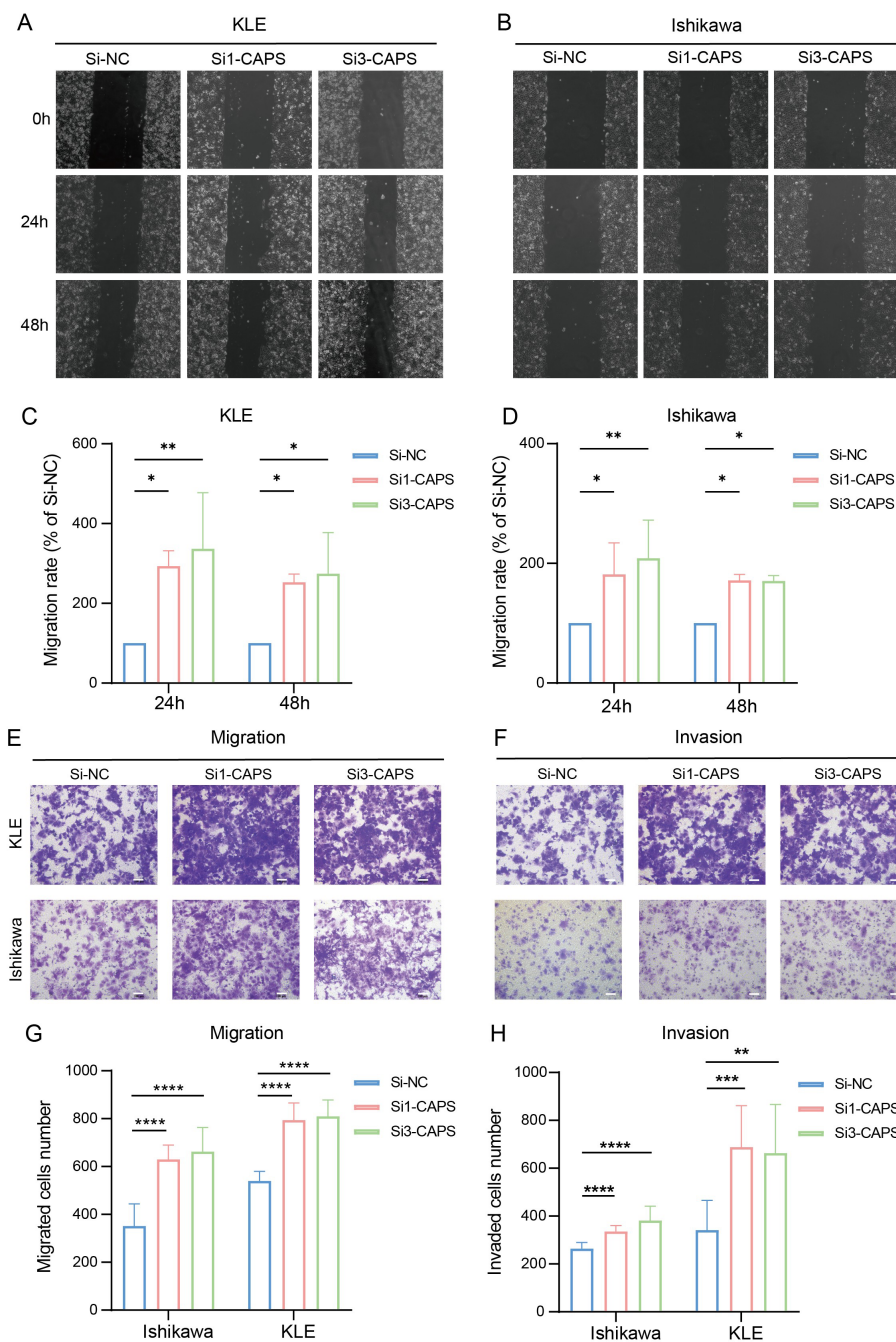


FIGURE 8

CAPS knockdown promotes migration and invasion of EC cells. (A, B) Wound healing assays evaluating the effect of CAPS knockdown on wound closure in KLE and Ishikawa cells. (C, D) Quantification of wound healing areas. (E, F) Transwell assays assessing the impact of CAPS knockdown on cell migration (E) and invasion (F) in KLE and Ishikawa cells. (G, H) Quantification of migrated (G) and invaded (H) cells in Transwell assays. (\* $P < 0.05$ , \*\* $P < 0.01$ , \*\*\* $P < 0.001$ , \*\*\*\* $P < 0.0001$ ).

proliferative reprogramming in diverse cancers. Consistently, our GSEA revealed that CAPS-high cells are enriched for ribosome biogenesis and OXPHOS, while classical proliferative pathways were suppressed—highlighting a metabolic phenotype divergent from the Warburg effect (22). This oxidative metabolic state is characteristic of terminally differentiated cells (23, 24). Prior research has shown that enhancement of OXPHOS can attenuate

proliferation and increase sensitivity to differentiation signals, supporting the notion that CAPS may modulate tumor cell fate via metabolic reprogramming (25). These insights may have therapeutic relevance, as targeting CAPS-associated metabolic states could offer novel strategies for inducing differentiation or suppressing proliferation in metabolically distinct EC subtypes.

Beyond its intrinsic cellular functions, CAPS also appears to influence the tumor microenvironment. Single-cell communication analyses revealed that CAPS-positive secretory epithelial cells engage in extensive and specific ligand-receptor interactions with multiple immune cell types, particularly through MDK-NCL and MIF-CD74 signaling axes (26). Among these, NK cells have been broadly associated with improved prognosis in solid tumors (27), while eosinophils may contribute to anti-tumor immunity by promoting T cell recruitment and remodeling of the tumor vasculature (28). Collectively, these findings suggest that CAPS exerts tumor-suppressive effects not only by modulating cellular metabolism and differentiation but also by shaping the immune microenvironment, thereby providing new insights into its multifaceted role in EC.

These observations suggest that CAPS may exert a dual tumor-suppressive effect-by modulating both epithelial cell behavior and the surrounding immune landscape. Accordingly, CAPS may serve as a potential biomarker for identifying immune-inflamed EC subtypes and guide immunotherapeutic stratification. Moreover, its downstream signaling pathways could represent viable targets for enhancing anti-tumor immune responses in EC.

Interestingly, previous studies have reported divergent roles for CAPS in other malignancies. For example, CAPS has been shown to promote glioma progression by activating the  $\text{Ca}^{2+}$ -ERK pathway (8) and to facilitate tumor growth in gastric and lung cancers (9). These discrepancies underscore the context-dependent nature of CAPS function, likely driven by tissue-specific molecular programs and microenvironmental influences. Our single-cell data suggest that CAPS expression is confined to a terminally differentiated epithelial subpopulation in EC, highlighting the limitations of bulk-tissue analyses, which may obscure functionally distinct cellular subsets. While previous studies have linked CAPS overexpression to stress-responsive or metabolically activated tumor states, our findings instead reveal an association with epithelial differentiation and suppression of proliferative capacity.

In summary, CAPS represents a promising molecule of prognostic and therapeutic relevance in endometrial carcinoma. Its elevated expression is consistently associated with more indolent pathological features and improved clinical outcomes, suggesting potential utility as a biomarker for patient stratification. Functionally, CAPS may exert tumor-suppressive effects by maintaining epithelial differentiation, restraining aberrant proliferation, and modulating the tumor immune microenvironment. Nevertheless, this study has several limitations. The single-cell RNA-seq analysis was derived from a single dataset (GSE173682) without cross-dataset validation, and the number of clinical samples used for validation was relatively small, consisting entirely of the endometrioid subtype. Future studies should incorporate molecular and histological stratification to enhance generalizability. In addition, functional assays were limited to *in vitro* models, and *in vivo* evidence and detailed mechanistic insights remain to be established. Future work will therefore focus on *in vivo* modeling, genetic rescue experiments, and cross-dataset single-cell validation to further elucidate the regulatory mechanisms and translational implications of CAPS in endometrial carcinoma and other malignancies.

## 5 Conclusion

This study identifies CAPS as a tissue-specific regulator exhibiting dual roles across malignancies. In EC, elevated CAPS expression is strongly associated with indolent pathological features and favorable clinical outcomes. Mechanistically, CAPS appears to function as a tumor suppressor by promoting epithelial differentiation and oxidative metabolism, inhibiting aberrant proliferation, and modulating the immune microenvironment. These findings support the clinical relevance of CAPS as a prognostic biomarker and highlight its potential as a therapeutic target in EC, offering a foundation for future mechanistic investigations and translational research.

## Data availability statement

The public datasets used in this study, including TCGA, GTEx, CPTAC, and GEO, are already deposited in their respective repositories and are openly accessible. No additional datasets requiring deposition were generated by the authors. The raw experimental data supporting the conclusions of this article will be made available by the authors without undue reservation.

## Ethics statement

The studies involving humans were approved by Ethics Committee of the First Hospital of Lanzhou University. The studies were conducted in accordance with the local legislation and institutional requirements. The participants provided their written informed consent to participate in this study.

## Author contributions

XC: Writing – original draft, Writing – review & editing, Conceptualization, Data curation, Software. RW: Formal Analysis, Methodology, Software, Writing – review & editing. ZW: Conceptualization, Data curation, Validation, Writing – review & editing. FW: Formal Analysis, Investigation, Writing – review & editing. DH: Software, Visualization, Writing – review & editing. XB: Funding acquisition, Project administration, Supervision, Writing – review & editing. XL: Project administration, Supervision, Writing – review & editing. YY: Project administration, Supervision, Writing – review & editing.

## Funding

The author(s) declare financial support was received for the research and/or publication of this article. This work was supported by the National Natural Science Foundation of China (No. 81960278) and the Joint Fund of Gansu Province (No. 25JRR1258).

## Conflict of interest

The authors declare that the research was conducted in the absence of any commercial or financial relationships that could be construed as a potential conflict of interest.

## Generative AI statement

The author(s) declare that no Generative AI was used in the creation of this manuscript.

Any alternative text (alt text) provided alongside figures in this article has been generated by Frontiers with the support of artificial intelligence and reasonable efforts have been made to ensure accuracy, including review by the authors wherever possible. If you identify any issues, please contact us.

## Publisher's note

All claims expressed in this article are solely those of the authors and do not necessarily represent those of their affiliated organizations, or those of the publisher, the editors and the reviewers. Any product that may be evaluated in this article, or claim that may be made by its manufacturer, is not guaranteed or endorsed by the publisher.

## Supplementary material

The Supplementary Material for this article can be found online at: <https://www.frontiersin.org/articles/10.3389/fimmu.2025.1688606/full#supplementary-material>

### SUPPLEMENTARY FIGURE 1

Kaplan-Meier survival analyses of CAPS across TCGA cancer types. (A) Colon adenocarcinoma (COAD); (B) Head and neck squamous cell carcinoma

(HNSC); (C) Kidney renal clear cell carcinoma (KIRC); (D) Lower-grade glioma (LGG); (E) Lung adenocarcinoma (LUAD); (F) Skin cutaneous melanoma (SKCM); (G) Thymoma (THYM); (H) Uterine corpus endometrial carcinoma (UCEC).

### SUPPLEMENTARY FIGURE 2

Multidimensional analysis of CAPS functional features. (A) Precise chromosomal localization of CAPS at 19q13. (B-C) GO and KEGG enrichment analyses of CAPS-associated genes. (D) GSEA-based pathway enrichment of CAPS-associated genes. (E) Correlation between CAPS expression and canonical immune checkpoint molecules. (F) Pan-cancer infiltration of 24 immune cell types estimated by ssGSEA. (G) Pan-cancer infiltration of 22 immune cell types estimated by CIBERSORT. (\*  $P < 0.05$ , \*\*  $P < 0.01$ , \*\*\*  $P < 0.001$ ). (Abbreviations: GO, Gene Ontology; KEGG, Kyoto Encyclopedia of Genes and Genomes; GSEA, Gene Set Enrichment Analysis; ssGSEA, single-sample GSEA.).

### SUPPLEMENTARY FIGURE 3

Single-cell RNA-seq analysis workflow and validation of CAPS expression features. A-B. Quality control of raw single-cell RNA-seq samples (A, before QC; B, after QC). C. Selection of HVGs. D. Elbow plot assessing PC significance. E. Seurat clustering resolution tree. F. UMAP two-dimensional embedding based on the top 15 PCs, partitioning all cells into 24 clusters. G. Proportional distribution of cell types across different patient samples. H. Bar plot showing the proportion of CAPS-positive cells. I. Secondary clustering of SecEC; UMAP displays 14 subclusters. J. Subclustering and functional annotation of secretory endometrial epithelial cells (SeECs) (Abbreviations: QC, quality control; HVG(s), highly variable gene(s); PC(s), principal component(s); UMAP, Uniform Manifold Approximation and Projection; SecEC, secretory epithelial cells.).

### SUPPLEMENTARY FIGURE 4

Correlations between CAPS expression and immune/stromal cell infiltration across TCGA pan-cancer cohorts. (A-K) Cancer-type-specific analyses-including BLCA, KIRC, and COAD-show the association between CAPS expression and estimated levels of immune and stromal infiltration.

### SUPPLEMENTARY TABLE 2

Clinical characteristics of EC samples from the GSE173682 single-cell RNA-seq dataset.

### SUPPLEMENTARY TABLE 3

Relative mRNA expression of CAPS in EC cell lines.

### SUPPLEMENTARY TABLE 4

Sequences of CAPS-targeting siRNAs and negative control.

## References

1. Siegel RL, Miller KD, Wagle NS, Jemal A. Cancer statistics, 2023. *CA Cancer J Clin.* (2023) 73:17–48. doi: 10.3322/caac.21763
2. Berek JS, Matias-Guiu X, Creutzberg C, Fotopoulou C, Gaffney D, Kehoe S, et al. FIGO staging of endometrial cancer: 2023. *J Gynecol Oncol.* (2023) 34:e85. doi: 10.3802/jgo.2023.34.e85
3. Khosravi GR, Mostafavi S, Bastan S, Ebrahimi N, Gharibvand RS, Eskandari N. Immunologic tumor microenvironment modulators for turning cold tumors hot. *Cancer Commun (Lond).* (2024) 44:521–53. doi: 10.1002/cac2.12539
4. Kumar H, Deshwal A, Datwani S, Li Z. Decoding high-grade endometrial cancer: A molecular-histologic integration using the cancer genome atlas framework. *J Clin Trans Pathol.* (2025). doi: 10.14218/JCTP.2025.00021
5. Shao W, Wang Q, Wang F, Jiang Y, Xu M, Xu J. Abnormal expression of calyphosine is associated with poor prognosis and cell biology function in colorectal cancer. *Onco Targets Ther.* (2016) 9:477–87. doi: 10.2147/OTT.S92226
6. Li F, Zhu D, Yang Y, Wu K, Zhao S. Overexpression of calyphosine is associated with poor prognosis in esophageal squamous cell carcinoma. *Oncol Lett.* (2017) 14:6231–7. doi: 10.3892/ol.2017.6973
7. Yang M, Sun Y, Sun J, Wang Z, Zhou Y, Yao G, et al. Differentially expressed and survival-related proteins of lung adenocarcinoma with bone metastasis. *Cancer Med.* (2018) 7:1081–92. doi: 10.1002/cam4.1363
8. Zhu Z, Wang J, Tan J, Yao YL, He ZC, Xie XQ, et al. Calyphosine promotes the proliferation of glioma cells and serves as a potential therapeutic target. *J Pathol.* (2021) 255:374–86. doi: 10.1002/path.5776
9. El Housni H, Lecocq R, Christophe D. Production of dog calyphosine in bacteria and lack of phosphorylation by the catalytic subunit of protein kinase A *in vitro*. *Mol Cell Endocrinol.* (1997) 135:93–7. doi: 10.1016/S0303-7207(97)00183-4
10. Daily NJ, Boswell KL, James DJ, Martin TF. Novel interactions of CAPS (Ca2+-dependent activator protein for secretion) with the three neuronal SNARE proteins required for vesicle fusion. *J Biol Chem.* (2010) 285:35320–9. doi: 10.1074/jbc.M110.145169
11. GTEx Consortium, Stranger BE, Dermitzakis ET, Sabatti C, Lappalainen T, and GTEx Project Team, et al. The genotype-tissue expression (GTEx) project. *Nat Genet.* (2013) 45:580–5. doi: 10.1038/ng.2653
12. Gordon M, Lumley T. forestplot: Advanced forest plot using 'grid'graphics. *R Package version.* (2017) 1:70. doi: 10.32614/CRAN.package.forestplot
13. Iasonos A, Schrag D, Raj GV, Panageas KS. How to build and interpret a nomogram for cancer prognosis. *J Clin Oncol.* (2008) 26:1364–70. doi: 10.1200/JCO.2007.12.9791
14. Calandra T, Roger T. Macrophage migration inhibitory factor: a regulator of innate immunity. *Nat Rev Immunol.* (2003) 3:791–800. doi: 10.1038/nri1200



15. Revelle WR. *psych: Procedures for personality and psychological research*. Evanston, IL: Northwestern University (2017).
16. Yu G, Wang LG, Han Y, He QY. clusterProfiler: an R package for comparing biological themes among gene clusters. *Omics*. (2012) 16:284–7. doi: 10.1089/omi.2011.0118
17. Newman AM, Liu CL, Green MR, Gentles AJ, Feng W, Xu Y, et al. Robust enumeration of cell subsets from tissue expression profiles. *Nat Methods*. (2015) 12:453–7. doi: 10.1038/nmeth.3337
18. Korsunsky I, Millard N, Fan J, Slowikowski K, Zhang F, Wei K, et al. Fast, sensitive and accurate integration of single-cell data with Harmony. *Nat Methods*. (2019) 16:1289–96. doi: 10.1038/s41592-019-0619-0
19. Jin S, Guerrero-Juarez CF, Zhang L, Chang I, Ramos R, Kuan CH, et al. Inference and analysis of cell-cell communication using CellChat. *Nat Commun*. (2021) 12:1088. doi: 10.1038/s41467-021-21246-9
20. Setu B, Nie Q, Echele G, Spencer SA. Calcyphosine is a microtubule-associated protein required for spindle formation and function. *bioRxiv*. (2023) 12:29.573632. doi: 10.1101/2023.12.29.573632
21. Jamal MH, Nunes ACF, Vaziri ND, Ramchandran R, Bacallao RL, Nauli AM, et al. Rapamycin treatment correlates changes in primary cilia expression with cell cycle regulation in epithelial cells. *Biochem Pharmacol*. (2020) 178:114056. doi: 10.1016/j.bcp.2020.114056
22. Papaneophytou C. The warburg effect: is it always an enemy? *Front Biosci (Landmark Ed)*. (2024) 29:402. doi: 10.31083/j.fbl2912402
23. Polito MP, Romaldini A, Rinaldo S, Enzo E. Coordinating energy metabolism and signaling pathways in epithelial self-renewal and differentiation. *Biol Direct*. (2024) 19:63. doi: 10.1186/s13062-024-00510-0
24. Park WY, Montufar C, Zaganjor E. Mitochondrial substrate oxidation regulates distinct cell differentiation outcomes. *Trends Cell Biol*. (2025) 35:274–7. doi: 10.1016/j.tcb.2025.02.004
25. van den Ameele J, Brand AH. Neural stem cell temporal patterning and brain tumour growth rely on oxidative phosphorylation. *Elife*. (2019) 8:e47887. doi: 10.7554/eLife.47887
26. Yu X, Xie L, Ge J, Li H, Zhong S, Liu X. Integrating single-cell RNA-seq and spatial transcriptomics reveals MDK-NCL dependent immunosuppressive environment in endometrial carcinoma. *Front Immunol*. (2023) 14:1145300. doi: 10.3389/fimmu.2023.1145300
27. Zhang S, Liu W, Hu B, Wang P, Lv X, Chen S, et al. Prognostic significance of tumor-infiltrating natural killer cells in solid tumors: A systematic review and meta-analysis. *Front Immunol*. (2020) 11:1242. doi: 10.3389/fimmu.2020.01242
28. Grisaru-Tal S, Dulberg S, Beck L, Zhang C, Itan M, Hediye-Zadeh S, et al. Metastasis-entrained eosinophils enhance lymphocyte-mediated antitumor immunity. *Cancer Res*. (2021) 81:5555–71. doi: 10.1158/0008-5472.CAN-21-0839